Received: 4 October 2021 | Revised: 2 November 2021 | Accepted: 2 November 2021

DOI: 10.1002/pro.4229

FULL-LENGTH PAPER

Three-dimensional structure of xylonolactonase from *Caulobacter crescentus*: A mononuclear iron enzyme of the 6-bladed β-propeller hydrolase family

Johan Pääkkönen[1] | **Nina Hakulinen**[1] | **Martina Andberg**[2] | **Anu Koivula**[2] | **Juha Rouvinen**[1]

[1]Department of Chemistry, University of Eastern Finland, Joensuu, Finland

[2]VTT Technical Research Centre of Finland Ltd, Espoo, Finland

Correspondence
Juha Rouvinen, Department of Chemistry, University of Eastern Finland, P.O. Box 111, FI-80101 Joensuu, Finland.
Email: juha.rouvinen@uef.fi

Funding information
This work received support from the Academy of Finland through the following projects: SA-IV4SP (Decision Number 118573), SA-ENGBIOCAT (grant numbers 287241 and 288677) and PENTOX (grant number 322610) projects.

Abstract

Xylonolactonase *Cc* XylC from *Caulobacter crescentus* catalyzes the hydrolysis of the intramolecular ester bond of D-xylonolactone. We have determined crystal structures of *Cc* XylC in complex with D-xylonolactone isomer analogues D-xylopyranose and (R)-(+)-4-hydroxy-2-pyrrolidinone at high resolution. *Cc* XylC has a 6-bladed β-propeller architecture, which contains a central open channel having the active site at one end. According to our previous native mass spectrometry studies, *Cc* XylC is able to specifically bind Fe^{2+}. The crystal structures, presented here, revealed an active site bound metal ion with an octahedral binding geometry. The side chains of three amino acid residues, Glu18, Asn146, and Asp196, which participate in binding of metal ion are located in the same plane. The solved complex structures allowed suggesting a reaction mechanism for intramolecular ester bond hydrolysis in which the major contribution for catalysis arises from the carbonyl oxygen coordination of the xylonolactone substrate to the Fe^{2+}. The structure of *Cc* XylC was compared with eight other ester hydrolases of the β-propeller hydrolase family. The previously published crystal structures of other β-propeller hydrolases contain either Ca^{2+}, Mg^{2+}, or Zn^{2+} and show clear similarities in ligand and metal ion binding geometries to that of *Cc* XylC. It would be interesting to reinvestigate the metal binding specificity of these enzymes and clarify whether they are also able to use Fe^{2+} as a catalytic metal. This could further expand our understanding of utilization of Fe^{2+} not only in oxidative enzymes but also in hydrolases.

KEYWORDS

Caulobacter crescentus, crystal structure, enzyme mechanism, hydrolase, iron, metal coordination, metalloenzyme, xylonolactonase, β-propeller hydrolase

Abbreviations: asu, asymmetric unit; *Cc*, *Caulobacter crescentus*; DLS, Diamond Light Source; ESRF, European Synchrotron Radiation Facility; HPD, (R)-(+)-4-hydroxy-2-pyrrolidinone; PON, paraoxonase; SMP30, senescence marker protein 30; XylB, xylose dehydrogenase; XylC, xylonolactonase; XylD, xylonate dehydratase.

1 | INTRODUCTION

Pentoses, the five-carbon sugars (in particular D-xylose and L-arabinose), are abundant in nature and can be found in large amounts in biomasses such as grasses, crops, and hardwoods and are consequently promising raw materials for the production of bio-based chemicals. The investigation of microbial metabolic pathways has revealed a number of enzymes, which can participate in the processing and modifying of pentose sugars. The oxidative pathway, called Dahms pathway, is utilized to convert an abundant pentose carbohydrate, D-xylose, to pyruvate and glycolaldehyde. In the first step, D-xylose is oxidized to D-xylonolactone by D-xylose dehydrogenase.[1] In the second step of the pathway, D-xylonolactone is hydrolyzed to D-xylonic acid.

D-Xylonolactone is also prone to being slowly hydrolyzed non-enzymatically to D-xylonic acid, but it has been reported that xylonolactonase improves the D-xylonolactone hydrolysis and thus production of D-xylonic acid both in in vivo and in vitro pathway studies.[1–3] Furthermore, in bacteria, the genes coding for the Dahms pathway enzymes are often arranged in one operon, which further suggests that the lactonase is needed for an efficient conversion of the xylonolactone to xylonic acid.[4] D-Xylonolactone exists as two isomers, D-xylono-1,5-lactone (D-xylono-δ-lactone) and D-xylono-1,4-lactone (D-xylono-γ-lactone). The two isomers of D-xylonolactone are likely to interconvert via a bicyclic intermediate described in References 5–7. Only D-xylono-1,4-lactone is available commercially, which may indicate difficulties in isolation of D-xylono-1,5-lactone.

Xylonolactonase (E.C. 3.1.1.68) catalyzes the hydrolysis of the intramolecular ester bond of D-xylonolactone (Figure 1a). The lactonase *Cc* XylC gene is found in *C. crescentus* bacterium in the same operon as the *Cc* XylB dehydrogenase and *Cc* XylD dehydratase enzymes. Thus, it can be assumed that the real substrate for *Cc* XylC is D-xylonolactone. In solution, D-xylose exists almost completely either in α-D-xylopyranose (34%) or β-D-xylopyranose (64%) diastereoisomeric forms.[8] The oxidation of the pyranose form results in D-xylono-1,5-lactone, which is probably the substrate for *Cc* XylC. This is also supported by the observation[9] that the structurally very similar D-glucono-1,5-lactone is also a substrate for *Cc* XylC.

We have recently discussed that divalent metal ions (such as Ca^{2+}, Zn^{2+}, and Fe^{2+}) are able to promote the non-enzymatic isomerization of D-xylono-1,4-lactone to D-xylono-1,5-lactone and thus improve the enzymatic hydrolysis to xylonic acid (Figure 1a).[1,9] The hydrolysis of its ester bond produces D-xylonic acid, which has a rather low pK_a (about 3.65),[10] which leads to acidification of the medium. The decrease of pH has often been used in in vitro lactonase assays to monitor enzymatic activity.

So far, detailed enzymatic characterization of xylonolactonases has been very limited. We have previously studied the *Cc* XylC, which was found on the basis of amino acid sequence homology to have a 6-bladed β-propeller fold.[1,3,11] In addition, we have recently found that *Cc* XylC unexpectedly binds to a single Fe^{2+} ion with high specificity and affinity and not, for example, to Ca^{2+} or Zn^{2+}.[9] Therefore, we have continued the analysis of *Cc* XylC by determining the three-dimensional structure of the enzyme to elucidate the binding of Fe^{2+} and its structural role in catalysis.

2 | RESULTS AND DISCUSSION

2.1 | Overall structure

We have determined three high-resolution crystal structures of the *Cc* XylC xylonolactonase (Table 1). Two structures were obtained in the presence of D-xylopyranose and represent two crystal forms, which have differences in ligand binding outside the active site. The third structure was obtained with (R)-(+)-4-hydroxy-2-pyrrolidinone ((R)-β-hydroxy-γ-butyrolactam, HPD, Figure 1b). The expressed polypeptide chain of the *Cc* XylC contained 290 amino acid residues. The mass spectrum analysis had previously shown that the initial methionine was cleaved,[9] and it was consequently absent in the crystallized protein material. The overall electron density maps were of good quality but there are weaker densities for the four first residues of the *Cc* XylC in one molecule in the asymmetric unit, indicating partial disorder in the N-terminus. The three-dimensional structures show that the *Cc* XylC is folded into a β-propeller protein[11] having six blades, that is, repeats of four-stranded antiparallel β-sheets. The blades are arranged around the central channel, which contains the active site at one end. The structure of the *Cc* XylC is rather regular without any larger insertions except one protruding loop with a short α-helix in blade 1. In addition, there is a 13-residue-long C-terminal polypeptide tail, which packs against the propeller and forms a cap over the central channel at the opposite end to the active site (Figure 2a).

2.2 | Crystal structures

The asymmetric units (asu) of the three *Cc* XylC crystal structures contained eight crystallographically independent monomers (2/asu + 4/asu + 2/asu) in total (Table 1). All of the structures had a strong electron

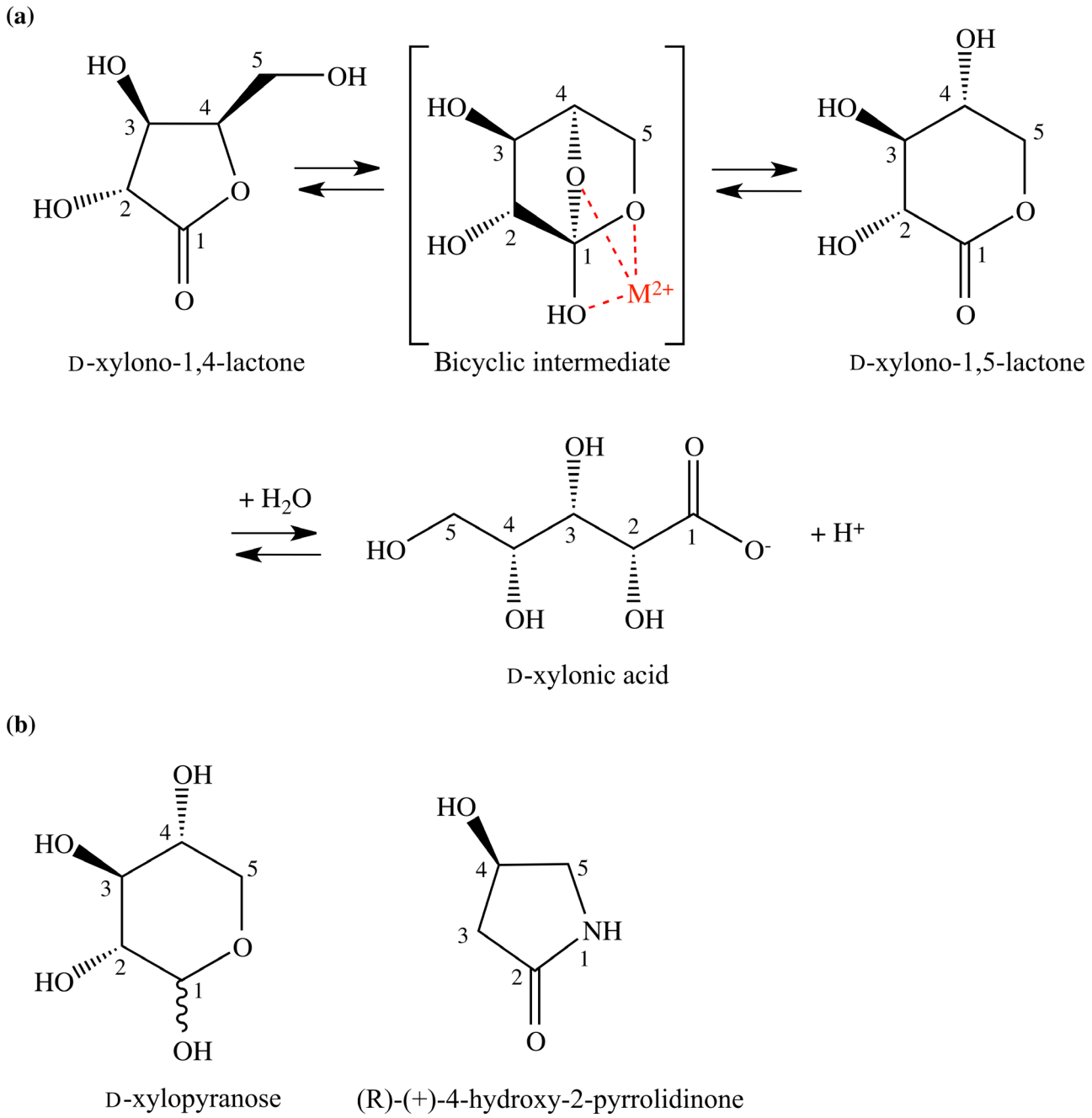

FIGURE 1 (a) The hydrolysis of D-xylonolactone, which is suggested to involve the isomerization reaction of D-xylono-1,4-lactone to D-xylono-1,5-lactone as the first step, which is catalyzed non-enzymatically by a divalent metal ion (M^{2+}). The lactonase-catalyzed hydrolysis reaction produces D-xylonic acid, which has relatively low pK_a (see also Figure 5). (b) The ligands successfully used as cryoprotectants and observed in the active site of the enzyme

density peak in the active site and were modelled as an Fe^{2+} ion according to our earlier native mass spectrometric studies.[8] The presence of the bound iron was also verified with native mass spectrometry from the protein crystals (Figure S1).

Two substrate analogues were observed in the complex structures. The molecular structure of D-xylopyranose (D-xylose) is very similar to that of D-xylono-1,5-lactone except that the pyranose ring has a hydroxyl substituent instead of a carbonyl group, and both ligands have a six-membered ring. Another substrate analogue used was a cyclic amide, HPD, which has a five-membered ring and an amide group thus representing an analogue of D-xylono-1,4-lactone. The two crystal structures complexed with D-xylopyranose had clear electron densities for bound D-xylopyranose (Figure S2A) in the active site

TABLE 1 X-ray data collection and refinement statistics

PDB ID	7PLB	7PLC	7PLD
Crystal form	Rectangle	Parallelogram	Rectangle
Ligand	D-Xylopyranose	D-Xylopyranose	(R)-(+)-4-Hydroxy-2-pyrrolidinone
Beamline	DLS i04-1	DLS i04-1	DLS i04-1
Wavelength (Å)	0.91587	0.91587	0.91587
Space group	$C\ 2\ 2\ 2_1$	$P\ 1\ 2_1\ 1$	$C\ 2\ 2\ 2_1$
a, b, c (Å)	85.8, 171.0, 79.1	45.8, 82.2, 159.2	87.7, 171.7, 79.2
α, β, γ (°)	90, 90, 90	90, 97.7, 90	90, 90, 90
Resolution (Å)	85.58–1.73 (1.79–1.73)	158.24–2.15 (2.23–2.15)	85.97–1.70 (1.76–1.70)
Observations	121,864 (11,959)	115,401 (11,849)	131,593 (12,969)
Unique observations	61,016 (6,025)	59,670 (6,048)	65,883 (6,493)
Completeness	100.0% (99.9%)	93.5% (95.2%)	99.7% (98.9%)
I/σ_I	9.2 (1.1)	3.9 (1.0)	9.2 (1.0)
$CC_{1/2}$	0.998 (0.564)	0.991 (0.660)	0.999 (0.538)
R_{merge}	0.049 (0.719)	0.100 (0.551)	0.048 (0.784)
R_{meas}	0.069 (1.017)	0.141 (0.779)	0.068 (1.109)
R_{work}	0.1807	0.1978	0.1936
R_{free}	0.2178	0.2502	0.2343
Number of protein monomers in the asymmetric unit	2	4	2
Number of protein atoms	4,504	8,829	4,457
Number of waters	553	611	579
Number of ligand atoms	147	89	86
Ramachandran favorable (%)	97.73	97.71	97.37
Ramachandran outliers (%)	0	0	0
Rms deviation in bond lengths (Å)	0.003	0.003	0.006
Rms deviation in bond angles (°)	0.692	0.630	0.815
Average B factor (Å^2)	28.34	28.58	27.30

in all six molecules (2/asu + 4/asu) of the asymmetric units. The D-xylopyranose molecules were bound as β-anomers in all enzyme structures in a very similar fashion. The equatorial O1 is bound to the Fe^{2+} ion with a short bond distance (2.0 Å) indicating strong binding to the metal cation. The binding can be considered as stereospecific for β-anomer and not for α-anomer, which has the O1 in an axial position, which would not allow the bond formation with Fe^{2+}. β-D-Xylopyranose also forms several hydrogen bonds with *Cc* XylC protein. O1 and O2 form hydrogen bonds with Asn101, O2 with Asn101 and Arg99, O3 and O4 with Glu120, and O5 with Asn146. In addition, Trp211 has a clear role in binding since it packs against the flat ring of D-xylopyranose (Figure 3a).

The crystal structure obtained with HPD showed electron densities (Figure S2B) for four ligand molecules in one *Cc* XylC molecule (chain B) and one in the other (chain A). One of the ligands was bound to the active site in the same site as D-xylopyranose and showed clear electron density that corresponds to a planar carbonyl group and atoms in α-positions. The rest of the molecule was disordered, probably because of multiple binding modes. The binding of the HPD was slightly tilted when compared to the binding of D-xylopyranose. The carbonyl oxygen was strongly bound to Fe^{2+} (distance 1.9 Å). There are also possibilities for hydrogen bonds between the HPD and Asn101 or Asp196 depending on the binding mode (Figure 3b). We modelled the binding mode of D-xylono-1,4-lactone to the active site by mimicking the

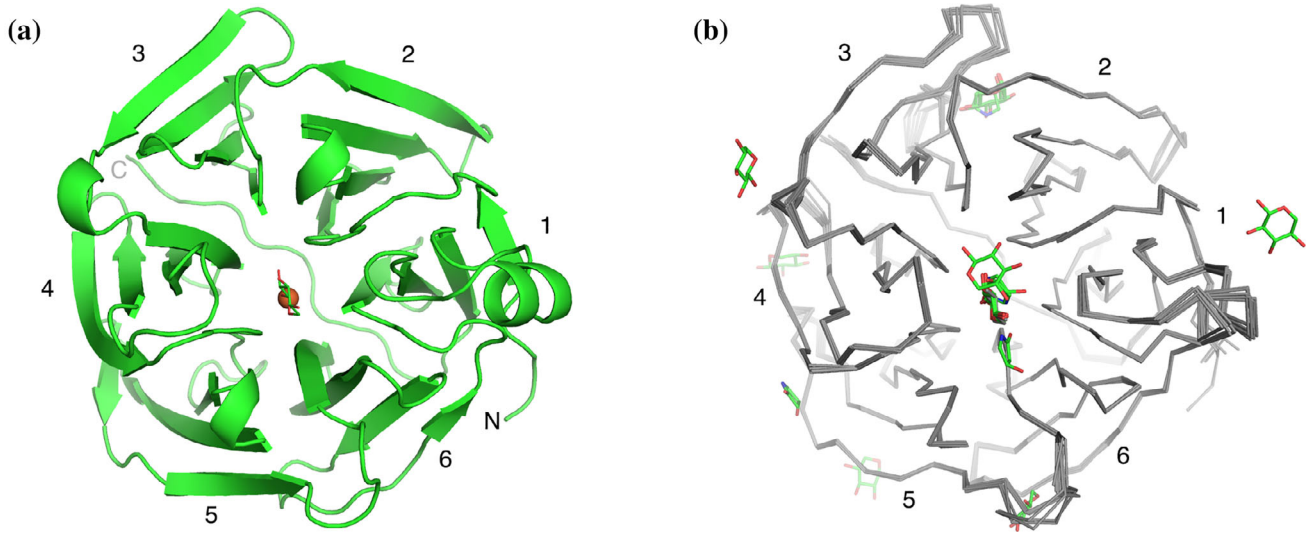

FIGURE 2 (a) The overall three-dimensional structure of the *Cc* XylC. The polypeptide chain of monomeric protein is presented as a green cartoon model. The blades of the β-propeller are numbered from 1 to 6. The bound Fe^{2+} ion in the central channel is shown as a brown ball and D-xylopyranose as a stick model. (b) The superimposed eight monomers from the three crystal structures are shown as grey ribbon chains. The additional bound ligand molecules are shown as green stick models

binding modes of D-xylopyranose and HPD (Figure 3e) and found several close contacts between the atoms of D-xylono-1,4-lactone and the side chains of the amino acid residues in the active site. D-Xylono-1,4-lactone has the C5 in an axial position, which renders its structure different to D-xylono-1,5-lactone, which has all substituents in equatorial positions. In consequence, it seems that *Cc* XylC prefers D-xylono-1,5-lactone as substrate over D-xylono-1,4-lactone.

In addition to the ligands bound to the active site, electron densities for ligands were observed in nine additional binding sites on the *Cc* XylC surface (Figure 2b). In most cases there was only one observed ligand binding among eight protein molecules. In the HPD complex structure, there was a second HPD molecule near the Fe^{2+}-bound HPD molecule. This second molecule packs against the flat face of bicyclic indole part of Trp211 (Figure 3b). This further supports the role of the side chain of Trp211 as binding to the flat face of cyclic carbohydrate molecules.

We found unexpectedly that one of the additional binding sites had electron densities for a ligand in four protein molecules. HPD binding was observed once in this site, and α-D-xylopyranose binding was observed in three structures. This binding site is located between blades 2 and 3 (Figure 2b), and it forms a clear pocket on the *Cc* XylC surface, although less deep compared to the active site pocket (Figure 4a, b). α-D-Xylopyranose forms hydrogen bonds from O3 to His23 of blade 2, and from O4 to Gly67 of blade 3 (Figure 4c). According to the crystal structures, the binding of α-D-xylopyranose seems to be stereospecific as we did not observe any density for O1 in the equatorial position, which would exist in the β-anomer of D-xylopyranose. It is possible that Trp28 from blade 2 restricts the binding of β-D-xylopyranose. There are significant alterations in the loop conformations upon ligand binding (Figure 4c). It is thus possible that this additional binding site would be an allosteric site for α-D-xylopyranose participating, for example, in regulation of the oxidative D-xylose pathway. However, we do not have any other experimental evidence supporting this suggestion, and it would also be challenging to study because D-xylopyranose exists in solution as a mixture of α- and β-anomers in which β-anomer binds to the active site and α-anomer to the surface pocket.

2.3 | Metal coordination

All the eight *Cc* XylC molecules in the crystal structures have a similar structural architecture for Fe^{2+} binding. There is a mononuclear Fe^{2+} center that is coordinated to six ligand atoms having an octahedral geometry. Fe^{2+} is coordinated to the side chains of Glu18 (blade 2), Asn146 (blade 5), and Asp196 (blade 6). There are three vacant sites, which are all occupied in the observed crystal structures. Two vacant sites are always occupied by water molecules, and the third site can be occupied by an oxygen of a substrate or, when a substrate or other ligand is not bound to the active site, by a water molecule (Figure 3). The structure without the bound ligand has three Fe^{2+}-coordinated water molecules. Two of them

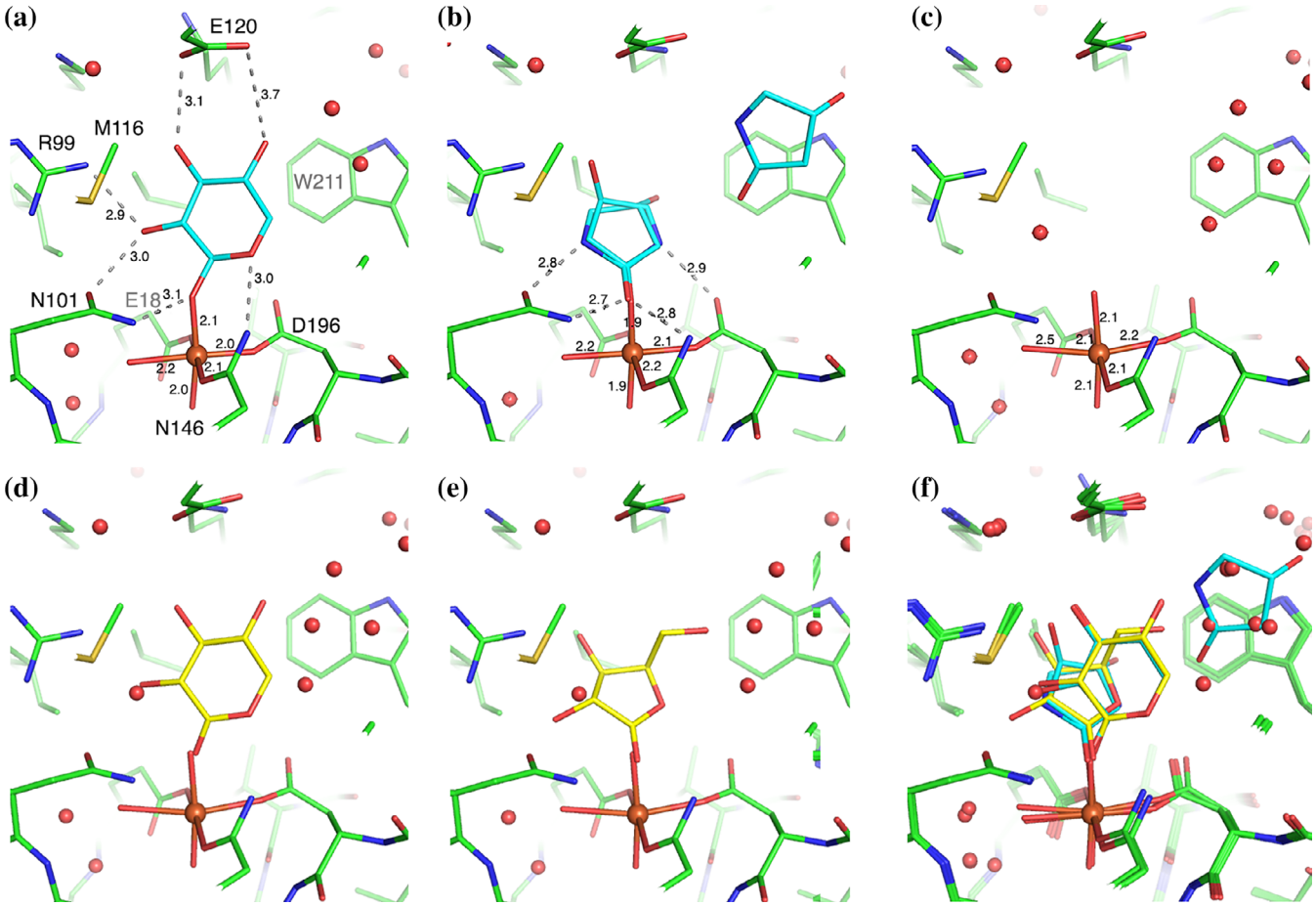

FIGURE 3 The active site and bound ligands. The protein structures are shown as green stick models and ligand structures as cyan stick models. Iron atoms and water oxygens are presented as balls in brown and red, respectively. The lengths of hydrogen bonds and coordination bonds are given in ångströms. The side chains from three amino acid residues (Glu18, Asn146, and Asp196), which are bound to the Fe^{2+}, are all in the same plane (planar triad). (a) The bound D-xylopyranose in the structure of the rectangular crystal, molecule A. (b) The bound HPD in the crystal structure, molecule B. (c) The active site without the ligand in the crystal structure with HPD, molecule A. (d) Modelled binding of D-xylono-1,5-lactone (in yellow) to the active site (same as in c). (e) Modelled binding of D-xylono-1,4-lactone (in yellow) to the active site (same as in c). (f) All three experimental structures superimposed together with the models of two isomers of D-xylonolactone (in yellow)

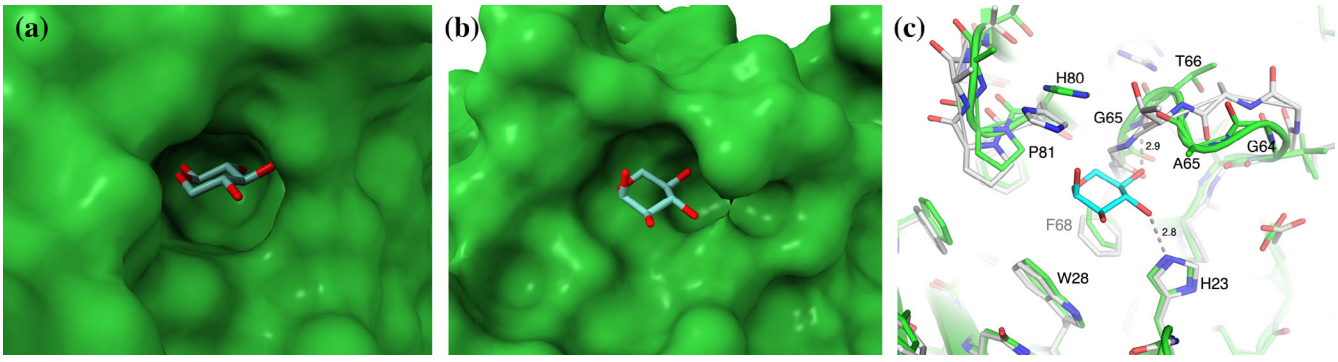

FIGURE 4 The binding of D-xylopyranose anomers to the *Cc* XylC. Ligands are shown as cyan stick models and protein surfaces in green. (a) β-D-Xylopyranose binding to the active site. (b) α-D-Xylopyranose binding to the putative allosteric site on the protein surface. (c) Details of the putative allosteric site. The protein atoms in complex with α-D-xylopyranose are in green, and without the ligand in grey

are strongly bound (distance 2.1 Å), whereas the third one has a longer distance (2.5 Å). The two strongly bound water molecules are probably the two water molecules, which were detected earlier in the native mass spectrum of the *Cc* XylC in the presence of Fe^{2+}[9] and also in the native mass spectrum by using a sample made of dissolved crystals (Figure S1).

The coordination of Fe^{2+} in the *Cc* XylC resembles to some extent the coordination of iron in other non-heme enzymes, such as mononuclear non-heme iron oxygenases.[12] These enzymes contain the so-called 2-His-1-carboxylate facial triad, where the Fe^{2+} is coordinated to three amino acid side chains, thus leaving three vacant positions for solvent or substrate atoms,[13] similarly to the *Cc* XylC. However, in the facial triad of the oxygenases, the three coordinating amino acids are located on one face of the metal cluster whereas in the *Cc* XylC structure the three coordinating amino acids are all in the same plane around the iron; the coordination of which could thus be called a "planar triad" (Figure 3). The differences in the binding geometries probably reflect different enzymatic activities. The enzymes having the facial triad are all oxidative enzymes capable of activating dioxygen, whereas the *Cc* XylC is a hydrolase.

2.4 | Reaction mechanism

According to the crystal structure, β-D-xylopyranose binds to the active site in a very defined manner in which O1 is coordinated to the catalytic Fe^{2+}. β-D-Xylopyranose can be considered as a competitive inhibitor and a substrate analogue. It is very well superimposable with the molecular model of D-xylono-1,5-lactone, thus providing a view on how the actual substrate would bind (Figure 3f). On the basis of the complex structures, we present a reaction mechanism in which the substrate, D-xylono-1,5-lactone, first binds to the Fe^{2+} (Figure 5). This increases the electrophilicity of the carbonyl carbon C1, so that a weak nucleophilic water can attack C1. The formed intermediate is then deprotonated, followed by the breaking of the ester bond, and finally the product, D-xylonic acid, is released. The proton exchange results in the final product, D-xylonate anion (Figures 1a and 5). The proposed reaction mechanism includes only one catalytically relevant interaction with the enzyme, the binding to Fe^{2+}. In fact, the crystal structures do not suggest any other putative amino acid residues, which would, for example, promote a nucleophilic attack of water to the carbonyl carbon. According to the literature, divalent metal ions

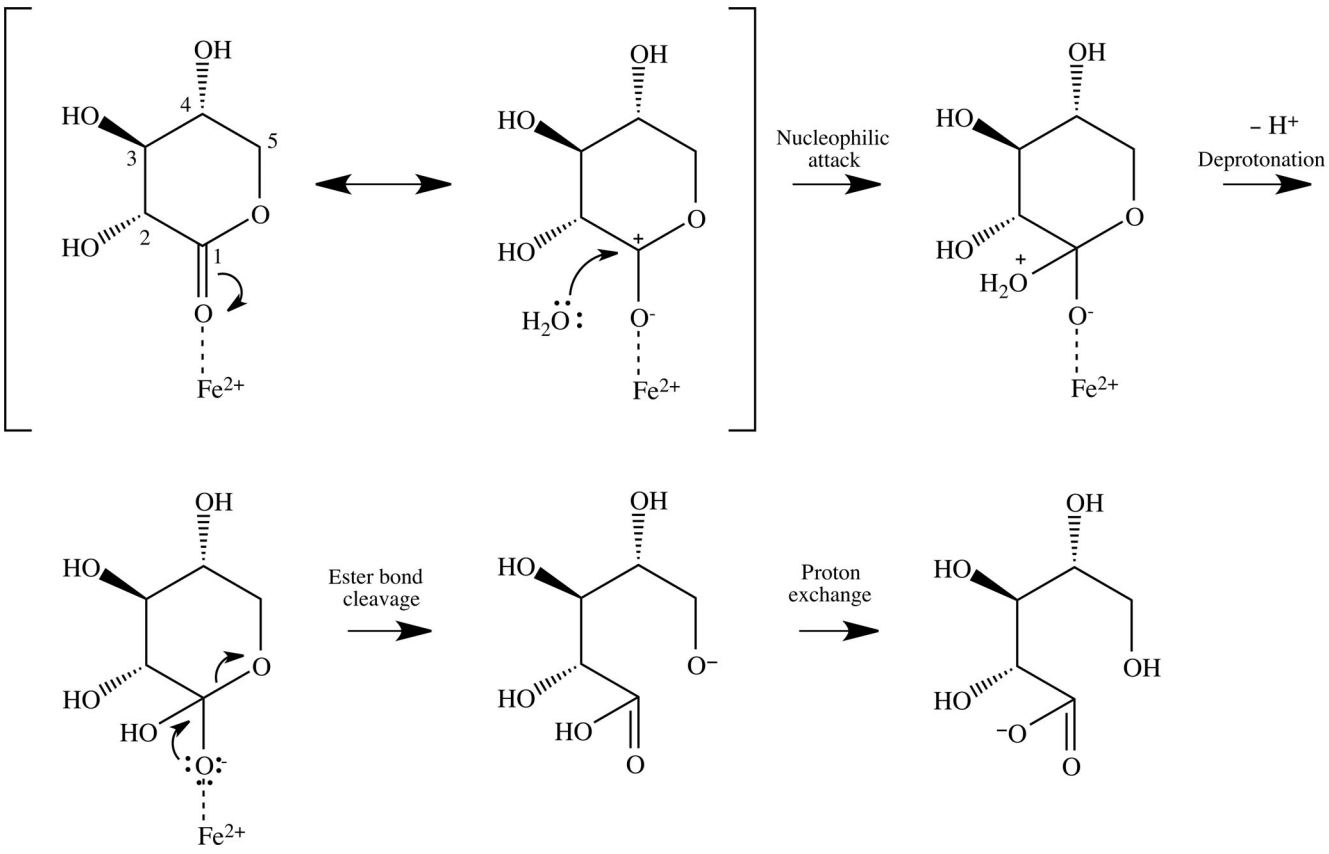

FIGURE 5 The proposed reaction mechanism for the *Cc* XylC catalyzed hydrolysis of D-xylono-1,5-lactone to form D-xylonic acid. See the text for more details

alone are able, at least weakly, to catalyze the ester bond hydrolysis.[13-16] Consequently, it might be possible that by the formation of a substrate–enzyme complex, the lifetime of otherwise weak association of Fe^{2+} and the carbonyl oxygen increases considerably in appropriate orientations. This in turn would allow a weak nucleophile, a water molecule, to attack and initiate the intramolecular ester bond hydrolysis reaction.

2.5 | 6-Bladed β-propeller hydrolase family

When homologous proteins were searched in the Protein Data Bank, we found in total eight enzymes, which showed amino acid sequence identities with the *Cc* XylC (Table 2). They all have a similar 6-bladed β-propeller fold, are hydrolases, and have a catalytic mononuclear metal ion (Figure 6a). The metal ion in the solved crystal structures is either calcium, magnesium, or zinc but not iron. The coordination of metal is similar among these enzymes (Figure 6b). A detailed comparison is presented in Figure 6c,d, which shows the metal binding in *Cc* XylC and mouse SMP30. When considering the metal coordination, all of the eight enzymes have coordinating amino acids in the same plane, but there are either three or four amino acids, which participate in metal ion binding (Figure 6b).

Three enzymes have about 30% amino acid identities with the *Cc* XylC, namely mouse and human senescence marker proteins (SMP30) and *Photinus pyralis* luciferin-regenerating protein. All these enzymes have three amino acids residues, which are bound to the metal cation (Table 2). The crystal structures have been determined for human and mouse SMP30. The biological role of SMP30 proteins has been vague, but it has been reported that they are able to hydrolyze various substrates such as D/L-glucono-δ-lactone, D/L-gulono-γ-lactone and D/L-galactono-γ-lactone and also to catalyze lactone-ring formation. The crystal structures for human and mouse SMP30 have been determined with several ligands such as 1,5-anhydro-D-glucitol,[17] which is bound approximately to the same position as the ligands in the crystal structures of the *Cc* XylC. The metal ion is coordinating to Glu18 (blade 2), Asn154 (blade 5), and Asp204 (blade 6), in a very similar manner as the Fe^{2+} in the *Cc* XylC. Another enzyme, which has three similar metal-coordinating residues (Glu18, Asn160, and Asp212), is the luciferin-regenerating enzyme, but its biological function is unclear.[18] This crystal structure does not contain any bound ligand in the active site. The protein was crystallized in presence of $MgCl_2$, and in consequence, the bound metal ion was interpreted as Mg^{2+}[19] (Figure 6b).

Four other 6-bladed β-propeller enzymes have a lower sequence identity with *Cc* XylC (Table 2), and they all have four amino acid residues participating in metal ion

TABLE 2 Representative crystal structures of 6-bladed β-propeller hydrolase family

Enzyme	Source	PDB	Resolution (Å)	Amino acids	Identity to *cc* XylC %	Active site metal	Metal coordinating amino acids	Ligand (substrate analogue)
Xylonolactonase	*Caulobacter crescentus*	7PLB	1.7	289	100	Fe^{2+}	E18, N146, D196	D-Xylopyranose
SMP30	Mouse	4GN8	1.7	299	30	Ca^{2+}	E18, N154, D204	1,5-Anhydro-D-glucitol
SMP30	Human	4GNC	1.8	299	29	Ca^{2+}	E18, N154, D204, D104	1,5-Anhydro-D-glucitol
Luciferin-regenerating enzyme	*Photinus pyralis*	5D9B	1.5	311	30	Mg^{2+}	E18, N160, D212	No
Gluconolactonase	*Xanthomonas campestris*	3DR2	1.7	305	19	Ca^{2+}	E48, N134, N191, D242	No
Drp35 gluconolactonase	*Staphylococcus aureus*	2DG1	1.7	333	14	Ca^{2+}	E48, D138, N185, D236, S237	No
Diisopropylfluoro-phosphatase	*Loligo vulgaris*	2GVW	1.7	314	14	Ca^{2+}	E21, N120, N175, D229	Dicyclopentyl phosphoramidate
Paraoxonase (PON)	*Oryctolagus cuniculus*	1V04	2.2	355	11	Ca^{2+}	E53, N168, N224, D269	No

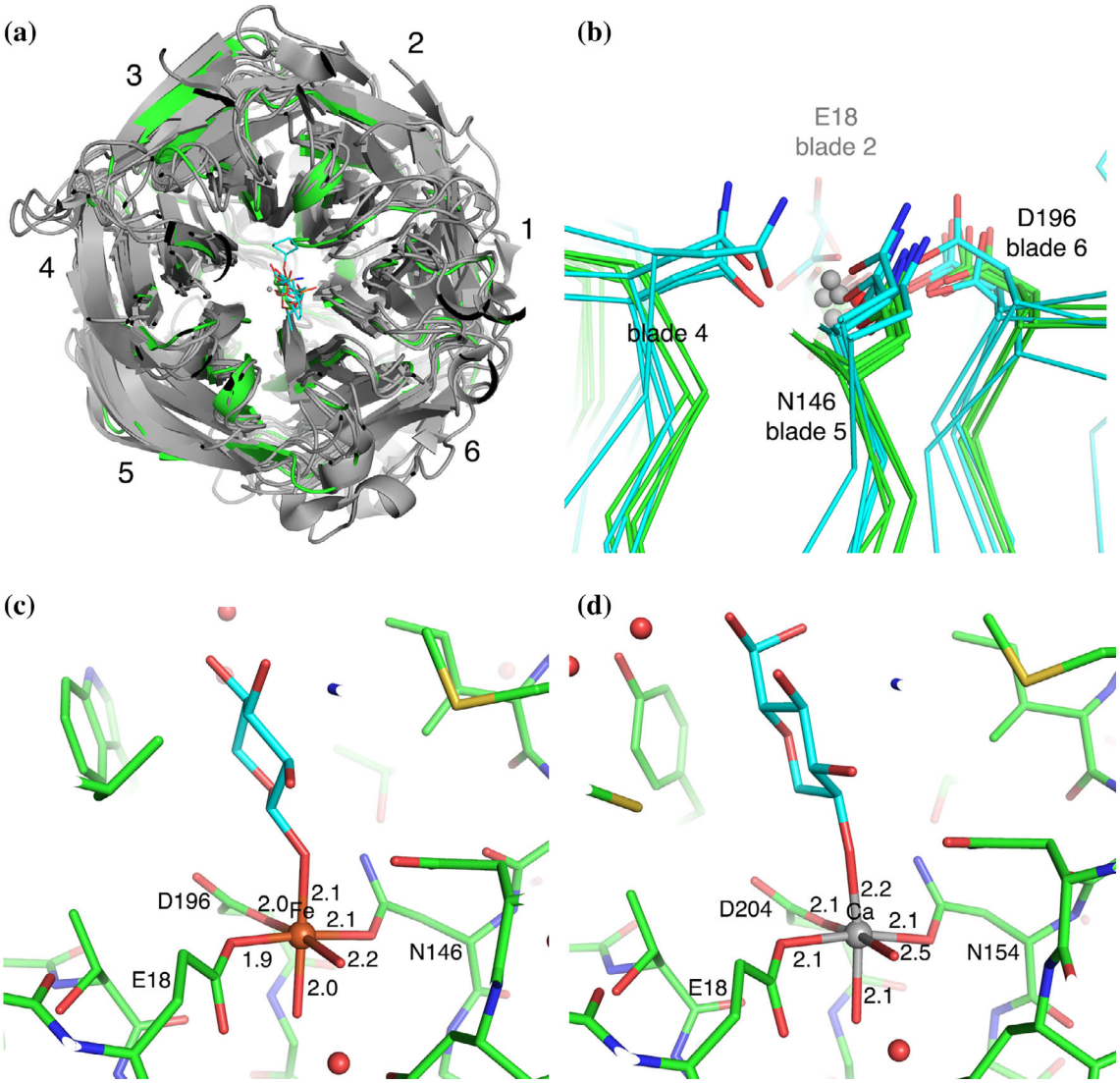

FIGURE 6 Superimposition of representative members (Table 2) of the 6-bladed β-propeller hydrolase family. (a) Cartoon representation of protein monomers. The *Cc* XylC is in green, other proteins are in grey. The active site ligands are shown as stick models. (b) The superimposition of metal coordination in active sites. The proteins that have three amino acids in plane, which participate in metal ion binding, are in green (xylonolactonase, mouse and human SMP30, and luciferin-regenerating enzyme), and proteins that have four amino acids in plane are in cyan (Drp35, gluconolactonase, diisopropylfluorophosphatase, and paraoxonase). The interacting residues in the *Cc* XylC are labelled as E18, D196, and N146. (c,d) The detailed comparison of coordination of catalytic metal ion in Cc XylC (c), and mouse SMP30 (d). The bond lengths between the metal ion and ligand atoms are given in ångströms. Carbon atoms of proteins are in green and of bound ligand (xylose in C, and 1,5-anhydro-D-glucitol in d) in cyan. Both crystal structures have been determined at 1.7 Å resolution. The comparison shows a clear resemblance in metal binding

binding (Figure 6b). The crystal structure of the gluconolactonase from *Xanthomonas campestris* has been determined at high resolution. The active site does not include bound ligand but contains Ca^{2+}, which is coordinated to four amino acid residues. Three of these coordinating amino acids can also be found in similar positions as in the *Cc* XylC, namely Glu48 (blade 2), Asn134 (blade 4), Asp242 (blade 6), and the fourth is an additional one, Asn191 (from blade 5). The corresponding asparagine (Asn101) in the *Cc* XylC structure is located further away from the Fe^{2+} (4.2 Å) to be able to coordinate to the iron. The crystal structure of *Staphylococcus aureus* Drp35 includes Ca^{2+} and similar coordinating residues Glu48, Asn185, and Asp236 as the *Cc* XylC does. Mutating any of these residues to alanine has been reported to result in an almost inactive enzyme.[19] Mutations Asn185Asp and Ser237Ala, on the other hand, led only to reduced activity, indicating that these non-conserved residues are not so critical for metal ion binding. *S. aureus* Drp35 has been suggested to belong to

paraoxonases, which act as lactonases but are also able to inactivate various organophosphates, including insecticides and nerve gases.[20] Diisopropyl fluorophosphatase from *Loligo vulgaris* is also able to hydrolyze organophosphorous nerve agents. Its crystal structure complexed with dicyclopentylphosphoramidate shows a coordination to Ca^{2+} by the oxygen of the phosphoramidate group of the substrate analogue. The metal ion has a similar coordination to four amino acid residues[21] as in the previously mentioned *X. campestris* gluconolactonase. Finally, the crystal structure of rabbit paraoxonase PON1 variant obtained by directed evolution has been determined to have a phosphate ion in the active site. The coordination of the Ca^{2+} ion is mediated by similar four coordinating amino acid residues as described above.[22]

3 | CONCLUSIONS

To our knowledge, the *Cc* XylC represents the first example of a hydrolytic enzyme having Fe^{2+} as a catalytic metal ion. As deduced from the complex structures, the major contribution to the ester bond hydrolysis is due to the coordination of carbonyl oxygen of the lactone ring to the enzyme-bound Fe^{2+}, which could promote a water molecule to attack the carbonyl carbon. The comparisons of the three-dimensional structure of the *Cc* XylC with other hydrolases from the 6-bladed β-propeller family showed that the metal ion coordination is highly conserved. This suggests that other members of this enzyme family could also utilize Fe^{2+} as a catalytic metal. However, verifying this would require further experimental studies. 6-Bladed β-propeller hydrolases, in general, show activity towards a wide range of substrates, such as esters, lactones, and phosphate esters. If the essential feature in catalysis requires only the coordination of the oxygen atom of a substrate to a divalent metal ion, there are more possibilities for variations in the active site structure. This would allow the utilization of members of this enzyme family to catalyze hydrolytic reactions with versatile substrates.

4 | MATERIALS AND METHODS

4.1 | Crystallization

The *Cc* XylC encoding gene was cloned into the linearized (*Nco*I and *Xho*I digestion) *Escherichia coli* pBAT4 expression vector. The N-terminal methionine codon was followed by an additional alanine codon, added to create a *Nco*I site. The expressed polypeptide chain of the *Cc* XylC thus contained 290 amino acid residues. The *Cc* XylC was produced and purified as a monomeric protein in a single anionic exchange chromatography step, as described earlier[1] and crystallized by using hanging drop vapor diffusion. For crystallization, approximately 20 M equivalents of $FeSO_4$ was added to the protein, and the solution was desalted with a PD-10 desalting column (GE Healthcare, Little Chalfont, England) and concentrated to about 8 mg/ml in 50 mM Tris buffer (pH 8.0). Drops were made by combining 1 μl protein and 1 μl precipitant solutions over 500-μl reservoirs, and crystallization plates were kept at 20°C after preparation. Initial screening was done with Crystal Screen by Hampton Research (HR2-110), and the best hits were obtained with high ammonium or lithium sulfate concentrations. Small, disordered crystals were obtained with 1.6 M $(NH_4)_2SO_4$ and 0.1 M HEPES (pH 7.5) as the precipitant solution. Streak seeding with a dog hair from these crystals at 1.6–1.8 M $(NH_4)_2SO_4$ yielded very small needle-like crystals. Another streak seeding or alternatively microseeding (drop diluted 1/320 with the precipitant solution used in drop preparation) from these microcrystals at 1.5 M $(NH_4)_2SO_4$ yielded clean two-dimensional rectangular crystals with rough maximum dimensions $200 \times 200 \times 10$ μm. Another crystal was also observed: when 2.0% (vol/vol) PEG400 and 0.05 M sodium malonate were used in addition to the 1.6 M $(NH_4)_2SO_4$ and 0.1 M HEPES (pH 7.5), clusters of parallelogram-shaped crystals were obtained. Streak seeding from these crystals in the same conditions yielded clean crystals with similar size as the rectangular crystals.

4.2 | X-ray crystallography

The crystals were transferred to cryoprotective solutions and stored in liquid nitrogen for X-ray crystallography measurements. The $(NH_4)_2SO_4$ concentrations used in crystallization were too high for the cryoprotective solution because it would precipitate when cooled down to 100 K, so 1.0 M $(NH_4)_2SO_4$ was used along with 0.1 M HEPES (pH 7.5) and 30% (wt/vol) cryoprotectant. In addition, with the parallelogram-shaped crystals, 2.0% (vol/vol) PEG400 was added as well. The crystals were unstable in the presence of most cryoprotectants, which were tried, including ethylene glycol, glycerol, and D-xylonolactone. However, they were stable with D-xylopyranose and HPD, which were conveniently also substrate analogues. The crystals were picked up in nylon loops, stored in liquid nitrogen and sent to be measured at the synchrotrons at European Synchrotron Radiation Facility (ESRF) and Diamond Light Source (DLS). All herein presented data were obtained at the i04-1 beamline at DLS, and an early dataset that resulted in the

first preliminary structure was measured at the ID30A-3 (MASSIF-3) beamline at ESRF.

4.3 | Structure determination

The first preliminary structure was calculated using the early dataset. The images were processed to 2.8 Å resolution with XDS program package,[23] and using this data file, calculations were done with PHENIX software suite.[24] Using the homologous mouse SMP30 gluconolactonase (PDB entry 4GN7)[16] as the initial model, molecular replacement was done with MR-Rosetta[25] and Phaser.[26] Extensive manual editing of the model with Coot[27] and structure refinement with phenix.refine[28] resulted in a model, which contained few water molecules and lacked any ligands but could be used as an initial model for future calculations.

For determining the high-resolution structures, datasets of three crystals were selected: rectangular with D-xylopyranose, parallelogram-shaped with D-xylopyranose, and rectangular with HPD. Autoprocessed data files from DLS with the best statistics – xia2-dials,[29–33] autoPROC[23,31–35] and autoPROC for the three datasets respectively—were selected and used in calculations. Molecular replacement was done with Phaser using the preliminary structure as the starting model, and structure refinement was done with phenix.refine. Geometry restraints were calculated for the HPD using eLBOW.[36] Water molecules were initially modelled automatically using the "Update waters" option and later examined manually. Fe^{2+} ions and identifiable ligands were also added manually and refined automatically, and their occupancies were also refined if they were significantly less than one. Weight optimization parameters were enabled for the final refinement rounds. To further verify the presence of HPD in the active site of the corresponding structure, a polder map[37] was also calculated, and it showed the expected strong intensity at most of the lactam ring (Figure S3).

4.4 | Mass spectrometry

To show that the bound iron was present in crystalline protein, a native mass spectrometry sample was made from the rectangular crystals. They were picked up in a nylon loop and transferred to fresh drops of crystallization solution where they were dissolved by adding water. After enough crystals were collected, the drops were combined and buffer-exchanged to 10 mM ammonium acetate using a PD-10 desalting column. Using a Solarix XR Fourier transform ion cyclotron resonance (FT-ICR) mass spectrometer (Bruker Daltonik GmbH, Bremen, Germany), a native mass spectrum was measured with the same parameters as in the previous work[9] but with 300 scans. A clean mass spectrum with signals of both apo- and holo-forms of the enzyme was obtained, the holo-form being dominant (Figure S1). When another sample was prepared similarly but by dissolving the crystals in 10 mM $FeSO_4$ solution before the buffer exchange and the spectrum was measured, the weak apo-signals disappeared and the holo-signals remained, as expected.

ACKNOWLEDGEMENTS

We thank Arja Kiema (VTT) for technical assistance in protein purification. The FT-ICR facility is supported by Biocenter Finland (FINStruct), Biocenter Kuopio, the European Regional Development Fund (grant number A70135) and the EU's Horizon 2020 Research and Innovation Programme (EU FT-ICR MS project; grant agreement ID 731077). We acknowledge the European Synchrotron Radiation Facility for provision of synchrotron radiation facilities.

CONFLICT OF INTEREST

The authors declare that they have no competing interests.

AUTHOR CONTRIBUTIONS

Johan Pääkkönen: Formal analysis (equal); investigation (equal); validation (equal); visualization (equal); writing – original draft (equal). **Nina Hakulinen:** Funding acquisition (equal); investigation (equal); resources (equal); writing – review and editing (equal). **Martina Andberg:** Investigation (equal); writing – review and editing (equal). **Anu Koivula:** Conceptualization (equal); funding acquisition (equal); investigation (equal); resources (equal); writing – review and editing (equal). **Juha Rouvinen:** Conceptualization (equal); funding acquisition (equal); investigation (equal); project administration (equal); supervision (equal); visualization (equal); writing – review and editing (equal).

DATA AVAILABILITY STATEMENT

The structural data are available in the RCSB Protein Data Bank under the accession numbers: 7PLB, 7PLC and 7PLD. Information on the natural protein is available under the UniProtKB Accession number A0A0H3C6P8.

ORCID

Johan Pääkkönen https://orcid.org/0000-0002-2772-3327

Nina Hakulinen https://orcid.org/0000-0003-4471-7188

Martina Andberg https://orcid.org/0000-0002-8021-9947
Anu Koivula https://orcid.org/0000-0002-7600-5700
Juha Rouvinen https://orcid.org/0000-0003-1843-5718

REFERENCES

1. Boer H, Andberg M, Pylkkänen R, Maaheimo H, Koivula A. *In vitro* reconstitution and characterisation of the oxidative D-xylose pathway for production of organic acids and alcohols. AMB Expr. 2019;9:48.
2. Buchert J, Viikari L. The role of xylonolactone in xylonic acid production by *Pseudomonas fragi*. Appl Microbiol Biotechnol. 1988;27:333–336.
3. Toivari M, Nygård Y, Kumpula E-P, et al. Metabolic engineering of *Saccharomyces cerevisiae* for bioconversion of D-xylose to D-xylonate. Metab Eng. 2012;14:427–436.
4. Stephens C, Christen B, Fuchs T, Sundaram V, Watanabe K, Jenal U. Genetic analysis of a novel pathway for D-xylose metabolism in *Caulobacter crescentus*. J Bacteriol. 2007;189:2181–2185.
5. Jermyn MA. Studies on the glucono-δ-lactonase of *Pseudomonas fluorescens*. Biochim Biophys Acta. 1960;37:78–92.
6. Ueberschär K-H, Blachnitzky E-O, Kurz G. Reaction mechanism of D-galactose dehydrogenases from *Pseudomonas saccharophila* and *Pseudomonas fluorescens*. Eur J Biochem. 1974;48:389–405.
7. Bierenstiel M, Schlaf M. δ-Galactonolactone: Synthesis, isolation, and comparative structure and stability analysis of an elusive sugar derivative. Eur J Org Chem. 2004;4:1474–1481.
8. Enslow KR, Bell AT. The role of metal halides in enhancing the dehydration of xylose to furfural. ChemCatChem. 2015;7:479–489.
9. Pääkkönen J, Penttinen L, Koivula A, et al. Xylonolactonase from *Caulobacter crescentus* is a mononuclear nonheme iron hydrolase. Biochemistry. 2021;60:3046–3049.
10. Hummel M, Leppikallio M, Heikkinen S, Niemelä K, Sixta H. Acidity and lactonization of xylonic acid: A nuclear magnetic resonance study. J Carbohydr Chem. 2010;29:416–428.
11. Chen CK-M, Chan N-L, Wang AH-J. The many blades of the β-propeller proteins: Conserved but versatile. Trends Biochem Sci. 2011;36:553–561.
12. Que L, Ho RYN. Dioxygen activation by enzymes with mononuclear non-heme iron active sites. Chem Rev. 1996;96:2607–2624.
13. Bruijnincx PCA, van Koten G, Klein Gebbink RJM. Mononuclear non-heme iron enzymes with the 2-His-1-carboxylate facial triad: Recent developments in enzymology and modeling studies. Chem Soc Rev. 2008;37:2716–2744.
14. Wells MA, Bruice TC. Intramolecular catalysis of ester hydrolysis by metal complexed hydroxide ion. Acyl oxygen bond scission in Co^{2+} and Ni^{2+} carboxylic acid complexes. J Am Chem Soc. 1977;99:5341–5356.
15. Fife TH, Przystas TJ. Divalent metal ion catalysis in the hydrolysis of esters of picolinic acid. Metal ion promoted hydroxide ion and water catalyzed reactions. J Am Chem Soc. 1985;107:1041–1047.
16. Fife TH, Pujari MP. Metal ion catalysis in the hydrolysis of esters of 2-hydroxy-1,10-phenanthroline: The effects of metal ions on intramolecular carboxyl group participation. Bioorg Chem. 2000;28:357–373.
17. Aizawa S, Senda M, Harada A, et al. Structural basis of the γ-lactone-ring formation in ascorbic acid biosynthesis by the senescence marker protein-30/gluconolactonase. PLoS One. 2013;8:e53706.
18. Hosseinkhani S, Zadeh EE, Sahebazzamani F, Ataei F, Hemmati R. Luciferin-regenerating enzyme crystal structure is solved but its function is still unclear. Photochem Photobiol. 2017;93:429–435.
19. Yamashita K, Pan D, Okuda T, et al. An isomorphous replacement method for efficient *de novo* phasing for serial femtosecond crystallography. Sci Rep. 2015;5:14017.
20. Tanaka Y, Morikawa K, Ohki Y, et al. Structural and mutational analyses of Drp35 from *Staphylococcus aureus*. A possible mechanism for its lactonase activity. J Biol Chem. 2007;282:5770–5780.
21. Blum M-M, Löhr F, Richardt A, Rüterjans H, Chen JC-H. Binding of a designed substrate analogue to diisopropyl fluorophosphatase: Implications for the phosphotriesterase mechanism. J Am Chem Soc. 2006;128:12750–12757.
22. Harel M, Aharoni A, Gaidukov L, et al. Structure and evolution of the serum paraoxonase family of detoxifying and antiatherosclerotic enzymes. Nat Struct Mol Biol. 2004;11:412–419.
23. Kabsch W. XDS. Acta Cryst. 2010;D66:125–132.
24. Liebschner D, Afonine PV, Baker ML, et al. Macromolecular structure determination using X-rays, neutrons and electrons: Recent developments in *Phenix*. Acta Crystallogr. 2019;D75:861–877.
25. DiMai F, Terwilliger TC, Read RJ, et al. Improved molecular replacement by density- and energy-guided protein structure optimization. Nature. 2011;473:540–543.
26. McCoy AJ, Grosse-Kunstleve RW, Adams PD, Winn MD, Storoni LC, Read RJ. *Phaser* crystallographic software. J Appl Cryst. 2007;40:658–674.
27. Emsley P, Lohkamp B, Scott WG, Cowtan K. Features and development of *Coot*. Acta Crystallogr. 2010;D66:486–501.
28. Afonine PV, Grosse-Kunstleve RW, Echols N, et al. Towards automated crystallographic structure refinement with *phenix.refine*. Acta Crystallogr. 2012;D68:352–367.
29. Winter G. *xia2*: An expert system for macromolecular crystallography data reduction. J Appl Cryst. 2010;43:186–190.
30. Winter G, Waterman DG, Parkhurst JM, et al. *DIALS*: Implementation and evaluation of a new integration package. Acta Crystallogr. 2018;D74:85–97.
31. Evans P. Scaling and assessment of data quality. Acta Crystallogr. 2006;D62:72–82.
32. Evans PR, Murshudov GN. How good are my data and what is the resolution? Acta Crystallogr. 2013;D69:1204–1214.
33. Winn MD, Ballard CC, Cowtan KD, et al. Overview of the *CCP*4 suite and current developments. Acta Crystallogr. 2011;D67:235–242.
34. Vonrhein C, Flensburg C, Keller P, et al. Data processing and analysis with the *autoPROC* toolbox. Acta Crystallogr. 2011;D67:293–302.
35. STARANISO. Cambridge, United Kingdom: Global Phasing Ltd, 2018.
36. Moriarty NW, Grosse-Kunstleve RW, Adams PD. Electronic ligand builder and optimization workbench (eLBOW): A tool

for ligand coordinate and restraint generation. Acta Crystallogr. 2009;D65:1074–1080.
37. Liebschner D, Afonine PV, Moriarty NW, et al. Polder maps: Improving OMIT maps by excluding bulk solvent. Acta Cryst. 2017;D73:148.

SUPPORTING INFORMATION

Additional supporting information may be found in the online version of the article at the publisher's website.

How to cite this article: Pääkkönen J, Hakulinen N, Andberg M, Koivula A, Rouvinen J. Three-dimensional structure of xylonolactonase from *Caulobacter crescentus*: A mononuclear iron enzyme of the 6-bladed β-propeller hydrolase family. Protein Science. 2022;31:371–83. https://doi.org/10.1002/pro.4229